Received: 26 November 2022 | Revised: 24 March 2023 | Accepted: 15 April 2023

DOI: 10.1002/app.54030

RESEARCH ARTICLE

Applied Polymer SCIENCE WILEY

Suppressed physical aging in PMMA-titanium oxide nanocomposites by controlling alignment of nanoparticles

Miao Huo[1] | **Mingchao Ma**[1] | **Yinuo Teng**[1] | **Yuhan Xiao**[1] | **Yunlong Guo**[1,2]

[1]University of Michigan – Shanghai Jiao Tong University Joint Institute, Shanghai Jiao Tong University, Shanghai, China

[2]Center for Solid-battery Research, Global Institute of Future Technology, Shanghai Jiao Tong University, Shanghai, China

Correspondence
Yunlong Guo, University of Michigan – Shanghai Jiao Tong University Joint Institute, Shanghai Jiao Tong University, Shanghai 200240, China.
Email: yunlong.guo@sjtu.edu.cn

Funding information
National Natural Science Foundation of China, Grant/Award Number: 2157408

Abstract

This study investigates the physical aging process of PMMA-TiO_2 nanocomposites with different particle alignments. By using an external electric field to control the alignment of TiO_2 particles, a uniform distribution of TiO_2 particles in PMMA is transformed into a micrometer-level pillar structure. The physical aging process is measured using differential scanning calorimetry, and the particle alignment is confirmed by microscopy. Comparison of the aging behavior of different samples shows that the addition of randomly distributed TiO_2 nanoparticles accelerates the aging rate of the material. However, when the nanoparticles are realigned into a pillar structure, the aging rate significantly decreases. Moreover, in our experimental time scale, a dual-relaxation mechanism of aging is observed in the PMMA/TiO_2 nanocomposites. This work highlights the importance of particle alignment and structure on the aging behavior of polymer nanocomposites, which could have implications for designing materials with improved stability in applications that require slow aging.

KEYWORDS

ageing, composites, differential scanning calorimetry (DSC)

1 | INTRODUCTION

Adding inorganic nanoparticles (NPs) into polymer matrix is a way widely used to tune mechanical, thermal, and electrical properties of the resulting nanocomposites.[1–5] Even a low fraction of NPs can lead to a large summation of interfacial areas. As a result, segmental dynamics of polymer molecules in vicinity of the interfaces is substantially perturbed, getting rise to dramatic changes of the glass transition temperature (T_g) and structural relaxation behavior.[6,7] Physical aging is a phenomenon that occurs in glassy materials, where they are usually unstable and gradually move toward their thermodynamic equilibrium states after being cooled below their glass transition temperature T_g. This process is also referred to as structure relaxation.[8–11]

Physical aging is of importance for practical applications, for instance, aging of polymers can lead to deterioration of their mechanical and chemical properties, reducing their functional lifetime.[6,12,13] The underlying mechanisms of aging involve complex physical and chemical processes, such as structural relaxation, chain scission, crosslinking, and oxidation. Understanding these mechanisms and developing effective strategies to suppress them can significantly enhance the durability and reliability of polymer materials. Several studies have explored methods to suppress this aging process in polymer materials. One approach is to incorporate NPs with attractive interfacial interactions with the polymer. Wetted interfaces between polymer and NPs are preferred, as shown in studies involving polystyrene (PS), poly (methyl methacrylate) (PMMA), and poly (2-vinyl pyridine) (P2VP) nanocomposites containing silica or alumina nanospheres.[14–16] Another method utilizes confinement effect to suppress aging response. For instance, the aging rate of PS layers

within layered films was reduced with decreasing layer thickness, due to the confinement from interfaces.[17]

Polymer nanocomposites are advanced materials that often have improved mechanical properties or unique functions that respond to stimuli or change of surrounding conditions. However, some studies have found that these materials can age fast due to interactions between the polymer and NPs, which leads to instability.[6,9,18] Therefore, it is important to develop methods to slow down the aging process while maintaining the advanced functions of the composites, yet these strategies are not well-established or practically implemented. Additionally, there is still a need for a better understanding of how the morphology of the fillers affects aging of the material over time and with changes in temperature.

In this study, we investigated the structural relaxation of polymer nanocomposites with NPs of fixed loading but different morphologies. We manipulated the aggregation of NPs using a direct-current (DC) electric field to form micron-scale patterns and measured the viscoelastic response during aging of the nanocomposite.[19] Applying electric field is not only an easy and cheap method to align electrical sensitive fillers,[20] and can also facilitate the annihilation of defects.[21] This rearrangement of NPs under electric fields changes the size, type, and distribution of interfaces between the NPs and polymer matrix, thus altering the confinement conditions of the polymer at the nano- or micro-length scale. Our goal was to compare the structural relaxation behavior of the polymer nanocomposites under different morphologies.

2 | MATERIALS AND METHODS

2.1 | Materials and sample preparation

The polymeric material used in this study was poly(methyl methacrylate) (PMMA) with a molecular weight M_w of 10,000 g/mol and a polydispersity index (PDI) of 1.677, which was purchased from Sigma-Aldrich LLC (Shanghai, China) and used without any further purification. The titanium dioxide (TiO_2) NPs with diameters between 10 and 20 nm were purchased from Macklin Inc. (Shanghai, China) and used without further modification. The TiO_2 NPs used were of the anatase type, with a dielectric constant of 37,[22] while the dielectric constant of PMMA is 3.7.[23]

To fabricate nanocomposite samples, a mixture of PMMA and NPs in a weight ratio of 20:1 was first prepared in a beaker. A 10 mL of acetonitrile was then added into the mixture and stirred for 1 h, followed by ultrasonic treatment for 0.5 h. The obtained suspension was transferred into an evaporating dish and placed in a fume hood for 24 h to obtain a white flake solid. The solid was subsequently placed in a vacuum oven at 70°C overnight to remove residual solvent. Finally, the oven temperature was tuned to 200°C for 0.5 h to obtain a white lumpy solid composite. The sample was named PMMA-15, as the volume fraction of TiO_2 NPs is ~1.5%.

The electric-field treatment was performed at 200°C, using the electrorheological accessory of a rheometer (Anton Paar, MCR302). Sample PMMA-15 was placed between two 25-mm parallel plates, the gap between the fixtures was set to 0.5 mm. Subsequently, the sample was heated to 200°C on the rheometer, at which a voltage of 1500 V was applied vertically to the parallel plates for 30 min. The electric field was then removed after cooling down to room temperature to obtain an E-field treated sample named PMMA-15-E. For use of control tests, neat PMMA samples were prepared by isothermal annealing in a vacuum oven at 200°C for 0.5 h to form solid chunks. The resultant colorless and transparent sample is denoted as neat PMMA.

2.2 | Characterization of structural relaxation

A differential scanning calorimetry (DSC, Shimadzu DSC-60 plus) was used to measure the enthalpy changes of the samples at various times during isothermal aging. In aging tests, a sample of 3–5 mg was weighed and sealed in an aluminum crucible. The sample was then heated to 150°C with a constant rate of 20°C/min and held for 10 min to remove residual stress. After that the sample was quenched to an aging temperature (T_a) with a cooling rate of 30°C/min. The aging temperature for polymer materials is the temperature at which the polymer undergoes physical aging, which is typically below its T_g. In this work, the samples were annealed at seven chosen temperatures, the aging temperatures are $T_g - 35°C$, $T_g - 30°C$, $T_g - 25°C$, $T_g - 19°C$, $T_g - 15°C$, $T_g - 10°C$, and $T_g - 5°C$.

Subsequently, the sample was annealed at T_a for a certain aging time (t_a) ranging from 300 to 19,200 s. After annealing, the sample was quenched to 40°C with a rate of 30°C/min, and then reheated to 150°C at 20°C/min. The aging response such as specific heat capacity (C_p) curve and the associated enthalpy change (ΔH_a), was obtained from the heat flow in the second heating process. The enthalpy recovery in reheating process after cooling at different rates was also measured to determine activation energy.[24,25] The difference of this test protocol

from the previous aging test is that before the second heating the sample was quenched to 40°C under different cooling rates ranging from 30 to 0.1°C/min.

Heat capacity and enthalpy revolution are the main properties investigated in thermal analysis.[16,26–29] The heat capacity can be obtained by the heat flow signal ($\frac{dQ}{dt}$),

$$C_p = \frac{1}{m}\frac{dQ/dt}{dT/dt}, \quad (1)$$

where m is the sample mass, and dT/dt is the heating rate, which is 20°C/min, during the thermal analysis.

The evolution of enthalpy during the annealing can be obtained by integrating the difference in C_p between the aged and unaged data in a certain range of temperature.

$$\Delta H_a = \int_{T_1}^{T_2} \left[C_{p,a}(T) - C_{p,u}(T)\right] dT, \quad (2)$$

where $C_{p,a}(T)$ and $C_{p,u}(T)$ are the values of heat capacity of the sample before and after aging, T_1 and T_2 are reference temperatures below and above T_g, respectively, at where the values of the heat capacity before and after aging are equal.

According to its definition, the fictive temperature (T_f), the hypothetical temperature at which a glass or amorphous solid would be in thermodynamic equilibrium with its surroundings, is calculated from the formula below,

$$\int_{T_1}^{T_f} \left(C_{pl}(T) - C_{pg}(T)\right) dT = \int_{T_1}^{T_2} \left(C_p - C_{pg}(T)\right) dT \quad (3)$$

where T_1 and T_2T_2 are the reference temperatures below and above T_g, C_{pl}, and C_{pg} are liquid and glassy heat capacities, respectively.

Activation energy (Δh) can be estimated from the relaxation process with different cooling rates since a lower cooling rate results in denser glass. Therefore, overshoots are observable in heat capacity curves.[30] The activation energy can be obtained from,

$$\Delta h = -R\frac{d(\ln|q_1|)}{d\left(\frac{1}{T_f}\right)}, \quad (4)$$

where q_1 is the cooling rate.[30]

Subsequently, the corresponding $1/T_f$ is plotted as the function of cooling rate, and $\frac{\Delta h}{R}$ is estimated based on the slope of the linear fit under logarithmic coordinates.

3 | RESULTS AND DISCUSSION

Figure 1 shows the optical images of neat PMMA, PMMA-15, and PMMA-15-E. Prior to morphological measurements, the samples were cut into small pieces of rectangular solid and tilted properly to expose planes of the original surface and the cross section. Neat PMMA is colorless and transparent (Figure 1a), while the PMMA-15 an opaque black solid, as the TiO_2 NPs well dispersed in the composite largely scatter the incident light (Figure 1b). In PMMA-15-E, NPs agglomerate to form multiple cone-shaped clusters which are separated from each other by a distance of 500–1000 μm. The micro strips of NPs were formed under electric field and were retained after cooling to room temperature. The reason for the unsymmetrical distribution of NPs from one side to another may be that particles like TiO_2 have a density of 3.97 g/cm^{-3},[31] whereas the PMMA matrix has a density of 1.18 g/cm^{-3}.[32] Owing to gravity, this density contrast leads to the asymmetric distribution of the particles and their arrangement in the films.[33]

Due to the high-temperature and high intensity of electric field during the preparation of the samples, there is possibility for oxidation and chemical aging of PMMA in the samples. In order to prevent chemical aging from affecting the experimental results, Fourier transform infrared (FTIR) tests were conducted to determine whether there were significant differences in the chemical structure of the three samples. The FTIR analysis can be found in Figure S9 and Table S1. The results showed that no notable chemical aging was observed within the time scale studied in this work.

Figure 2 shows that the T_gs of neat PMMA, PMMA-15, PMMA-15-E are 108.2, 102.2, and 102.1°C, respectively, determined from the C_p curves. T_g, a second-order transition, was characterized by a step change of heat flow in the thermograms from the second heating process, as defined by Roos.[34] The midpoint of the change in slope was identified as the T_g of the system, by Ribeiro.[35] The glass transition temperatures of PMMA-15 and PMMA-15-E are quite close, while the T_g of neat PMMA is obviously higher than the others. Adding of NPs reduce the T_g of nanocomposites, similar phenomena were reported before and was attributed to non-wetting property between polymer and NPs.[36] A strong interfacial interaction between the matrix and filler can increase the T_g while a non-wetting interaction can decrease the T_g.

Figure 3 shows isothermal structural relaxation of neat PMMA when T_a ranges from $T_g - 35$°C to $T_g - 5$°C. More aging results at different temperatures can be found in Figures S1 and S2. In these relaxation experiments, the physical aging response of neat PMMA is observed as the endothermic overshoot of the heat capacity. As the aging

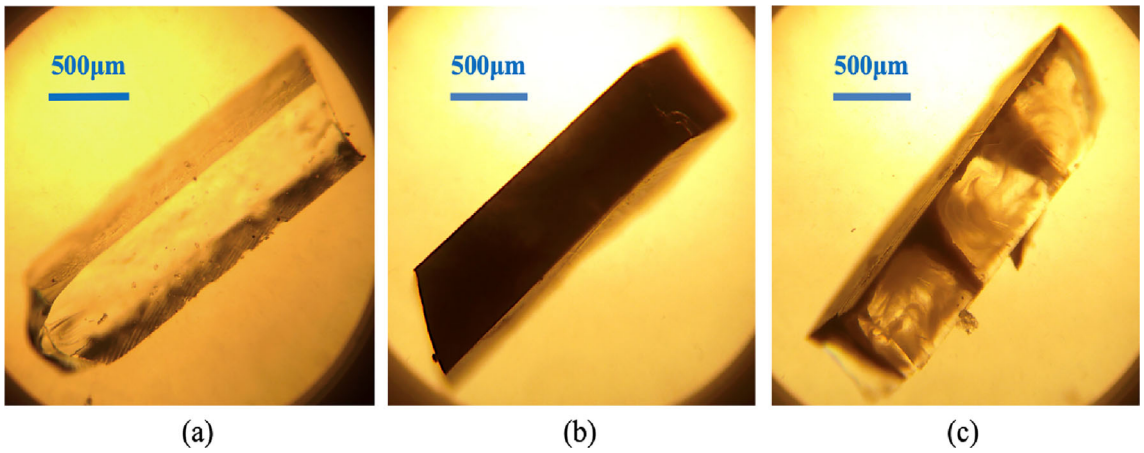

FIGURE 1 Samples used in the structural relaxation experiments. The images were taken by an optical microscope. (a) Neat PMMA, (b) PMMA-15, (c) PMMA-15-E, the black strips are fibrillated columns formed by the TiO_2 nanoparticles (NPs). [Color figure can be viewed at wileyonlinelibrary.com]

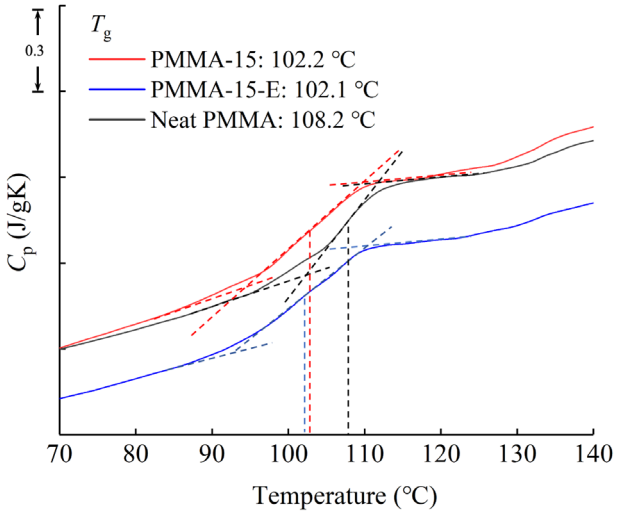

FIGURE 2 The heat capacity versus temperatures for neat PMMA, PMMA-15, and PMMA-15-E. T_g is determined from the midpoint of the cross-points of the linear fittings for the C_p data in glassy, transition, and liquid states. [Color figure can be viewed at wileyonlinelibrary.com]

time increases, the maximum value of the C_p overshoot increases and continuously shifts to a higher corresponding temperature. When $T_a = T_g - 35°C$ (Figure 3a), all the overshoots are wide and low. When the aging time is less than 19,200 s, the peaks can hardly be recognized on the C_p curve, but the departure from unaged curve can be identified. As the aging time increases, C_p increases as well. The C_p curves of all aging times are very close to each other, and the maximum values of these peaks are relatively low. This phenomenon may be caused by the large temperature difference between T_a and T_g. It takes a very long time for the material to gradually aged to a state causing a large magnitude of enthalpy decrease, since the molecular mobility is low at T_a. Therefore, under our experimental condition, the aging effect can be readily recovered without inducing conspicuous changes in the C_p curve.

When the aging temperature is increased by 5°C, at $T_a = T_g - 30°C$ (Figure 3b), the C_p overshoots increase significantly, which attributed to the increment of the mobility. When $T_a = T_g - 19°C$ (Figure 3c), the C_p overshoots are obvious under multiple aging time. The peak values are greatly improved compared to the previous temperatures. The result can be explained by the synergy between the driving force and the enthalpy span. It is noted that the enthalpy recovery depends on two factors.[37] One is the driving force, which increases with the increasing temperature; the other is the enthalpy span, which decreases with increasing temperature. Therefore, there will be a maximum in the enthalpy versus the aging temperature within a fixed experimental time scale.

When $T_a = T_g - 19°C$, the C_p overshoots become narrow and reach the highest height among all aging temperatures. Further increase the aging temperature to $T_a = T_g - 10°C$ (Figure 3d), the maximum value of the C_p curves begin to decline. The curves of 4800, 9600, and 19,200 s are very close to each other. At the same time, there is a noteworthy phenomenon, the overshoot position is obviously moving toward higher temperatures with the increasing of the aging temperature. When the aging temperature reaches $T_a = T_g - 5°C$ (Figure 3e), the C_p curves of all aging times overlap practically, demonstrate that the sample reaches the complete equilibrium state within a short period. The greatly reduced relaxation time is attributed to the improved molecular mobility at a temperature very close to T_g.

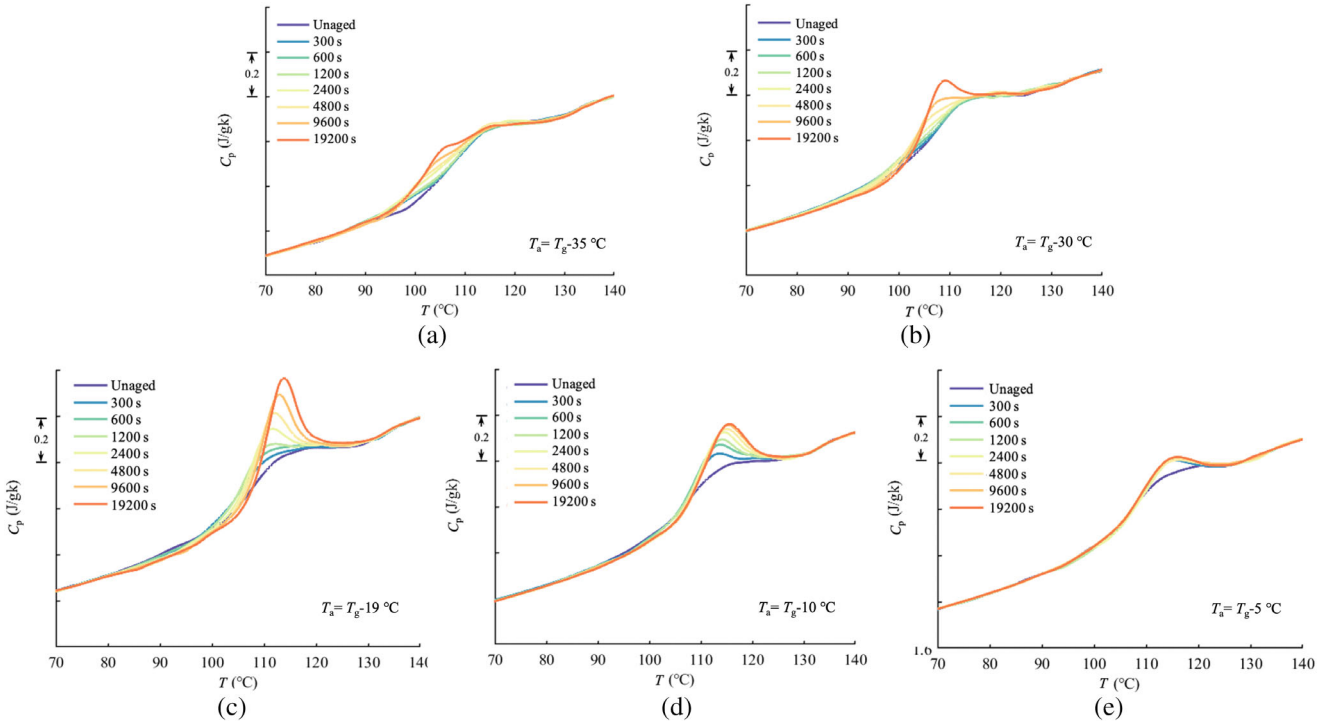

FIGURE 3 Heat capacity versus temperature of neat PMMA at (a) $T_a = T_g - 35°C$, (b) $T_a = T_g - 30°C$, (c) $T_a = T_g - 19°C$, (d) $T_a = T_g - 10°C$, (e) $T_a = T_g - 5°C$ after various aging times. [Color figure can be viewed at wileyonlinelibrary.com]

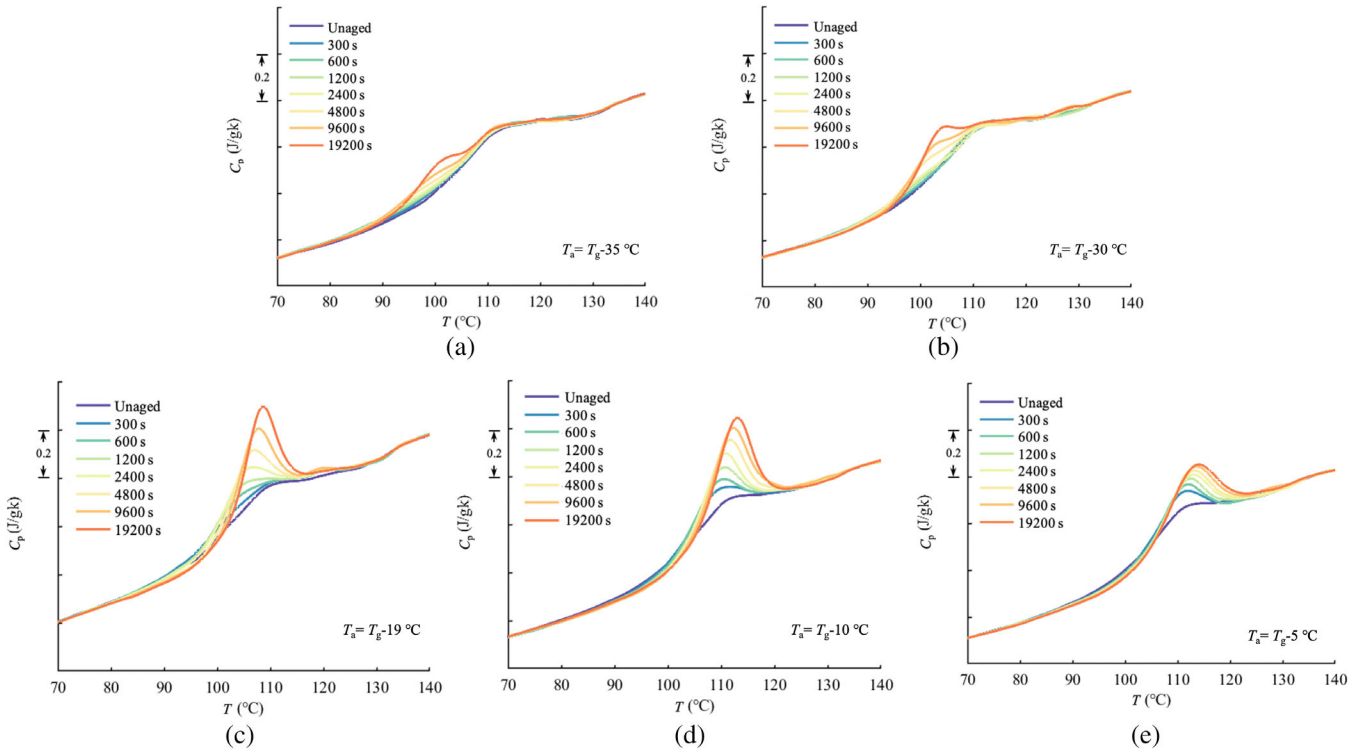

FIGURE 4 Heat capacity versus temperature of PMMA-15 at (a) $T_a = T_g - 35°C$, (b) $T_a = T_g - 30°C$, (c) $T_a = T_g - 19°C$, (d) $T_a = T_g - 10°C$, (e) $T_a = T_g - 5°C$ after various aging times. The error bar represents the SD of three duplicates. [Color figure can be viewed at wileyonlinelibrary.com]

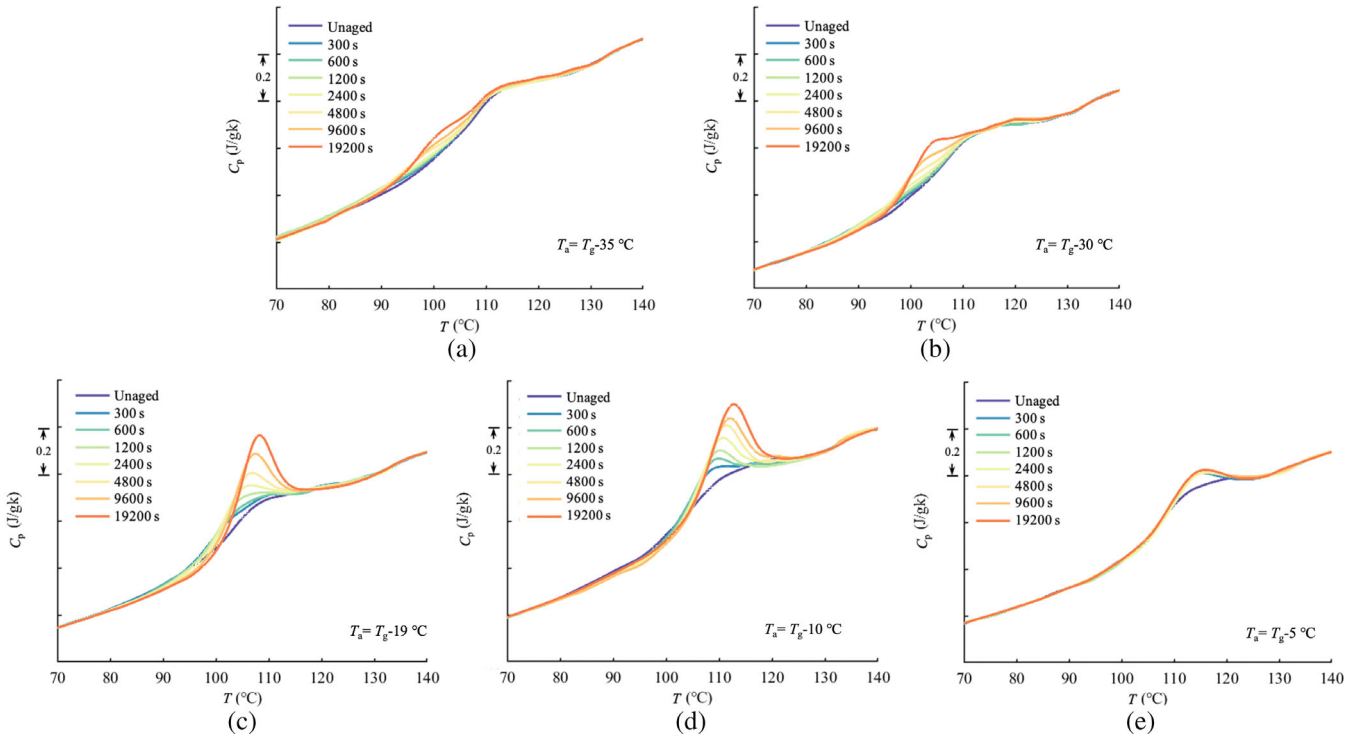

FIGURE 5 Heat capacity versus temperature of PMMA-15-E at (a) $T_a = T_g - 35°C$, (b) $T_a = T_g - 30°C$, (c) $T_a = T_g - 19°C$, (d) $T_a = T_g - 10°C$, (e) $T_a = T_g - 5°C$ after various aging times. The error bar represents the SD of three duplicates. [Color figure can be viewed at wileyonlinelibrary.com]

Figure 4 shows the isothermal relaxation of PMMA-15 when T_a ranges from $T_g - 35°C$ to $T_g - 5°C$. More thermograms at different temperatures can be found in Figures S3 and S4. Since the heat capacity of the TiO_2 NPs does not change during the annealing process, the observed overshoots of C_p are all considered to be caused by the PMMA matrix. The aging behavior of PMMA-15 is very similar to that of the neat PMMA. The overshoots of C_p first gradually increase with increasing temperature. After reaching the maximum value, the peak height then gradually decreases with increasing aging temperature. However, there are some different phenomena worth noting. When $T_a = T_g - 35°C$ (Figure 4a), the heat capacity overshoots of PMMA-15 are weaker than that of neat PMMA, that is, the overshoots are wide and low. The highest value of the aging peaks of PMMA-15 appears at $T_a = T_g - 19°C$ (Figure 4c), which is higher and thinner than that of neat PMMA. When $T_a = T_g - 10°C$ (Figure 4d), the C_p curves show an obvious decline. When $T_a = T_g - 5°C$ (Figure 4e), the aging behavior of PMMA-15 is very different from neat PMMA, embodied in C_p overshoots of PMMA-15 are separated from each other at all chosen aging temperatures. This difference demonstrated that the adding of NPs prolongs the process toward a complete equilibrium state.

Figure 5 shows the isothermal relaxation of PMMA-15-E when T_a ranges from $T_g - 35°C$ to $T_g - 5°C$. More thermograms at different temperatures can be found in Figures S5 and S6. At chosen aging temperatures, the heat capacity overshoot first gradually increases with increasing aging temperature. After reaching the highest value, the peak height decreases. Nonetheless, the aging behavior of PMMA-15-E exhibits noticeable differences from PMMA-15 in several aspects. When at $T_a = T_g - 35°C$ and $T_g - 30°C$ (Figure 5a,b), the heat capacity overshoot of PMMA-15-E is significantly lower than that of PMMA-15. At $T_a = T_g - 19°C$ (Figure 5c), the heat capacity overshoot reaches the highest value in PMMA-15-E, but the peak height is still lower than that of PMMA-15. When the aging temperature rises to $T_a = T_g - 5°C$ (Figure 5e), the C_p curves under all aging times have overlapped, which proves that PMMA-15-E reaches an equilibrium state within 300 s. Comparing the thermograms shown in Figures 3–5, the aging behavior of PMMA-15-E is surprisingly closer to that of the neat PMMA. After treated by an electric field, NPs in PMMA-15-E aggregated to form micron-scale columnar structures, so the interfaces between NPs and the polymer are significantly reduced. Therefore, the distance for the free volume holes' migration increases significantly, making PMMA-15-E relax like the bulk materials.

To compare the aging effect, Figure 6 exhibits the recovered enthalpy of neat PMMA, PMMA-15, and PMMA-15-E as a function of aging time. Recovered enthalpy at other temperatures can be found in Figures S7 and S8. The enthalpy is calculated using Equation (2). The solid line in

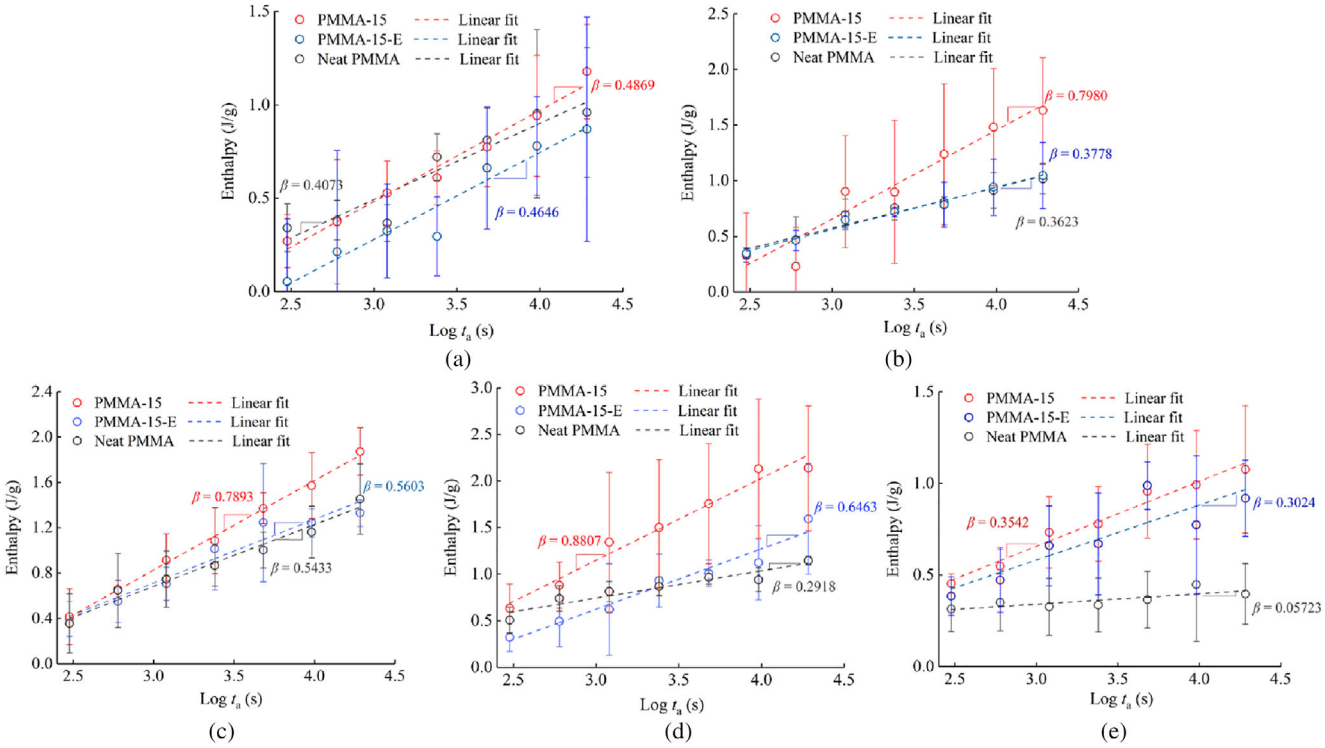

FIGURE 6 Relaxed enthalpy of neat PMMA, PMMA-15, and PMMA-15-E. The solid lines are linear fit of the data, and β is the slope of the fit line, which represents the aging rate. (a) $T_a = T_g - 35°C$, (b) $T_a = T_g - 30°C$, (c) $T_a = T_g - 19°C$, (d) $T_a = T_g - 10°C$, (e) $T_a = T_g - 5°C$. The error bar represents the standard deviation of three duplicates. [Color figure can be viewed at wileyonlinelibrary.com]

Figure 6 exhibits the linear fit of the data, and β is the slope of the fit line representing the aging rate. The largest aging rates of PMMA-15 and PMMA-15-E are captured at $T_a = T_g - 10°C$ (Figure 6d), while the largest aging rate of neat PMMA is found at $T_a = T_g - 19°C$ (Figure 6c). Among all chosen aging temperatures, the aging rate of PMMA-15 is the largest in all three samples. The aging rate of neat PMMA is slightly lower than that of PMMA-15-E. This phenomenon illustrates that adding TiO_2 NPs increases the surface areas in PMMA-15 greatly, which accelerates the aging process.[18] After treated by an electric field, NPs in PMMA-15-E are highly aggregated to form a micron-scale columnar structure. Therefore, the interfaces between NPs and the polymer are significantly reduced from PMMA-15, resulting in the reduction of the aging rate. In neat PMMA, the aging is relatively lower since there is no surface area created by NPs inside the bulk.[38]

Figure 7 depicts the aging rate and the recovered enthalpy ($T_a = 19{,}200$ s) of neat PMMA, PMMA-15, and PMMA-15-E as functions of ($T_g - T_a$). In Figure 7a, the aging rate of PMMA-15 is higher than the others at all aging temperatures. The aging rate of this sample is very low when $T_a = T_g - 35°C$, however, it gradually rises to a local maximum as the temperature rises. And then a peak valley appears between $T_a = T_g - 19°C$ and $T_a = T_g - 15°C$. When the temperature reaches $T_a = T_g - 10°C$, the aging rate arrives at another local maximum and then undergoes a rapid decline. The saddle-shaped aging rate shows a bimodal characteristic within the experimental aging temperature range.

The trend of the aging rate of PMMA-15-E is very similar to that of PMMA-15, also exhibiting a bimodal characteristic, but the overall value of the curve is greatly lower than that of PMMA-15, which is compatible with the previous literature.[39] When $T_a = T_g - 35°C$, the aging rate of PMMA-15-E is greater than at $T_a = T_g - 30°C$, this phenomenon may be ascribed to the large error bar range at low temperatures (as shown in Figure 6a). The Neat PMMA shows a very different aging rate characteristics from those of PMMA-15 and PMMA-15-E. The aging rate of neat PMMA rises continuously with the increasing of T_a to reach a maximum value near $T_a = T_g - 18°C$, and then decreases rapidly. The aging rate as a function of the temperature exhibits a unimodal feature within the experimental temperature range.

From the recovered enthalpy as a function of temperature in Figure 7b, a pattern very similar to the aging rate can be observed. PMMA-15 and PMMA-15-E show bimodal feature, while neat PMMA exhibits a unimodal

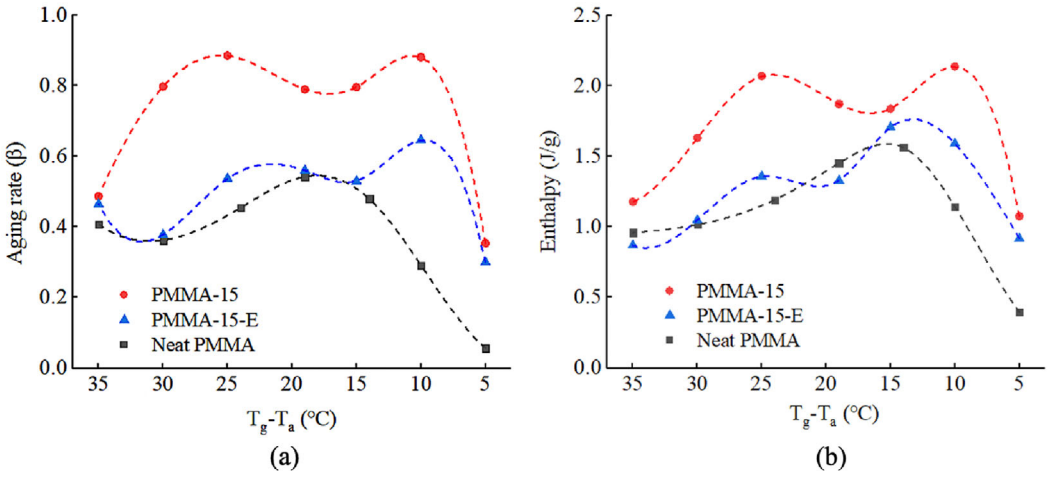

FIGURE 7 (a) Aging rate of neat PMMA, PMMA-15, and PMMA-15-E. (b) Enthalpy of neat PMMA, PMMA-15, and PMMA-15-E after aging for 19,200 s. The dash lines are calculated through cubic interpolation. [Color figure can be viewed at wileyonlinelibrary.com]

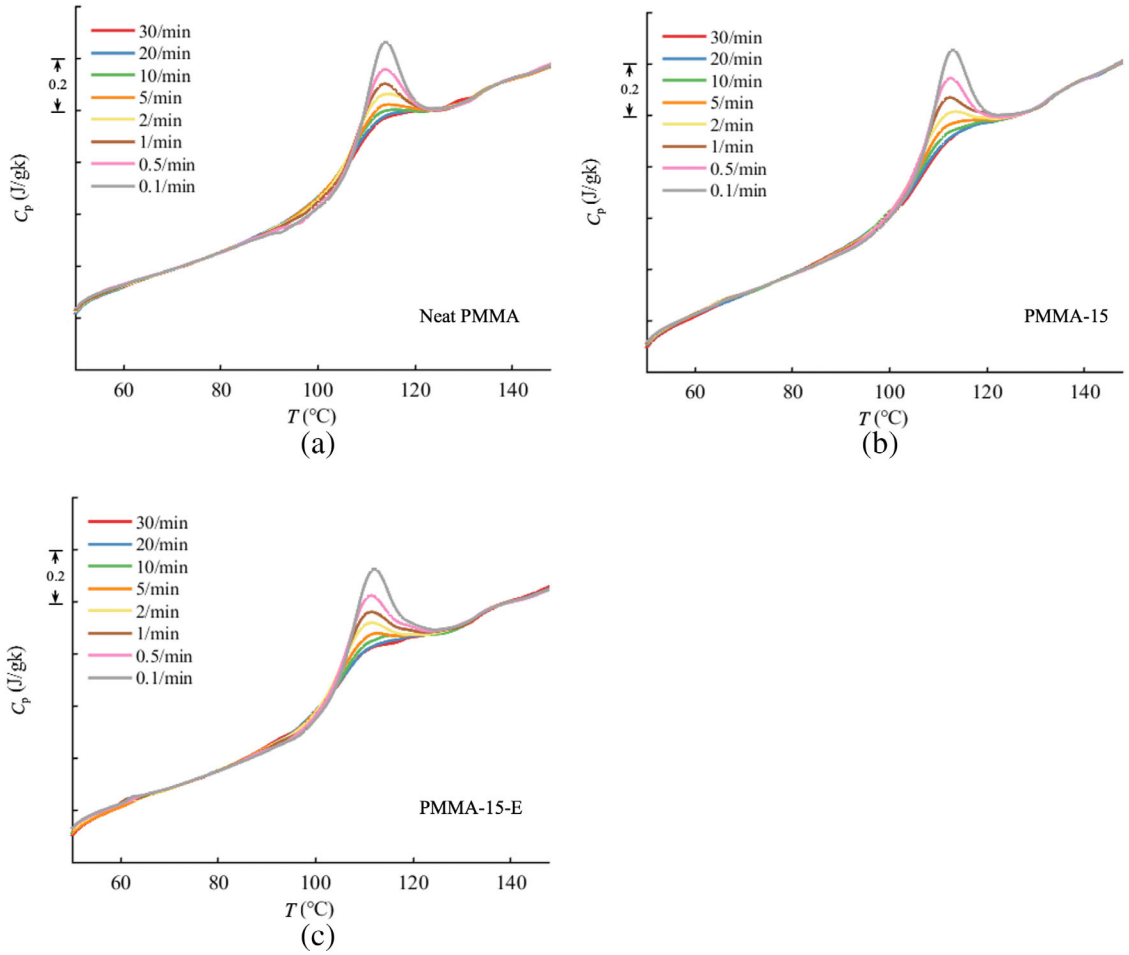

FIGURE 8 Heat capacity versus temperature of (a) neat PMMA, (b) PMMA-15, and (c) PMMA-15-E at different cooling rates. [Color figure can be viewed at wileyonlinelibrary.com]

feature within the experimental temperature range. The saddle shapes of the curves in Figure 7 may correspond to the coexistence of the two mechanisms in the structural relaxation process of polymers reported by Boucher.[39] The two mechanisms toward the equilibrium state not only appeared in the polymer thin films and

nanocomposites but also in some glassy metals. The mechanisms are of important significance to the studying of the materials' structural relaxation.[39,40] In the previous study of the mechanism of physical aging, there are two different process been found which follow different mathematical relationshiops[41,42]: one is the fast mechanism, which displays Arrhenius temperature dependence with low activation energy; while the other is the slow mechanism, which follows the super-Arrhenius temperature dependence.[43]

For the neat PMMA, only one peak appears in Figure 7, since the fast recovery mechanism is thickness dependent and compatible with the assumption of the diffusion of the free volume holes toward surfaces.[44–47] This hypothesis proposes that the continuous aging of the polymer in the glass state is caused by the free volume holes' migration over time. Neat PMMA is only affected by a small surface area, since the sample used in this work is a bulk material. Therefore, the migration distance of the free volume holes is vast. It is difficult to observe the fast recovery process in our experimental time scale. In contrast, for PMMA-15, the adding of NPs produces a large number of interfaces. Compared with neat PMMA, the distance required for the free volume holes to migrate to the interface is greatly reduced. Consequently, it takes less time to reach the equilibrium state, described as the time shorten effect.[41] The two mechanisms toward the equilibrium state can be observed within a short time. As such, the overall aging rate of PMMA-15 becomes higher than that of neat PMMA.[39] This can be explained by that the fast mechanism is related to the distance of the free volume holes' migration.

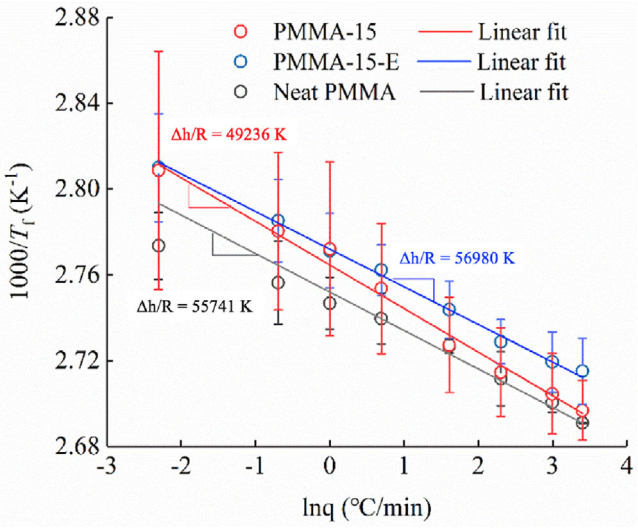

FIGURE 9 Relationship between fictive temperature and cooling rate of neat PMMA, PMMA-15, and PMMA-15-E. Values of $\Delta h/R$ are calculated by the slope of the fit lines. The error bars represent the standard deviation of three duplicates. [Color figure can be viewed at wileyonlinelibrary.com]

As for PMMA-15-E, the NPs aggregate to form micron-level columnar structures after been treated by an electric field. A large part of the polymer matrix is no longer affected by the interfaces. There is a significant reduction of the surface areas. Therefore, the overall aging rate and the recovered enthalpy of PMMA-15-E are lower than those of PMMA-15, but still slightly higher than those of neat PMMA. However, it is worth noting that in PMMA-15-E, the appearance of the two mechanisms at higher temperatures can still be observed. It can be explained by the interfaces that remain in PMMA-15-E, which have a remarked impact on the migration of the free volume holes.

Figure 8 shows the thermograms in heating after cooling by a series of speeds. The samples were heated above T_g under a certain heating rate, and then quenched to 40°C under different cooling rates ranging from 30 to 0.1/min. The structural relaxation is manifested by the overshoot in the heat capacity curve, which grows larger as the cooling rate decreases. Lower cooling rates give the atoms or molecules more time to rearrange to keep liquid structure and reduce their volume before glass transition, resulting in a denser glas.[48,49]

The peak of PMMA-15 in Figure 8b is the highest overshoot. The peaks of neat PMMA and PMMA-15-E in panels (a) and (c) are similar. The activation energy can be obtained from these experiments using Equation (4).[30]

Figure 9 illustrates the relationship between the fictive temperature and the cooling rate, in which the fictive temperature is determined by applying Equation (3) to the data above. The activation energy is calculated from the slope of the linear fit in Figure 9. The values of $\Delta h/R$ are 55,741, 56,980 and 49,236 for neat PMMA, PMMA-15-E, and PMMA-15, respectively. The values of $\Delta h/R$ for neat PMMA and PMMA-15 are quite close, whereas that for PMMA-15 is obviously lower. As the activation energy is obtained, the fragility index of these samples can be calculated to decide the stability of the structure and the thermodynamic properties of the glass in the T_g range:

$$m = \Delta h/\left(2.302RT_g\right), \tag{5}$$

where m represents the fragility index. The results listed in Table 1 show that neat PMMA and PMMA-15-E have

TABLE 1 Fragility index and related parameters of neat PMMA, PMMA-15, and PMMA-15-E.

	$\Delta h/R$ (K)	T_g (K)	m
Neat PMMA	55,741	381	64
PMMA-15	49,236	375	57
PMMA-15-E	56,980	375	66

similar fragility index, suggesting that aggregated NPs in micron scale has no effect on the temperature dependence of the physical and mechanical properties near T_g. Simultaneously, PMMA-15 has the lowest fragility index among the three samples. The result indicates that PMMA-15 has weaker temperature dependence compared with the others.

4 | CONCLUSIONS

This article explored the influence of different internal structures on the structural relaxation behavior of polymer nanocomposites. The distribution of NPs in PMMA-TiO_2 nanocomposites was adjusted via a DC electric field. Through the DSC experiments, the T_g and physical aging have been observed. Adding TiO_2 NPs (volume fraction of NPs = 1.5%) reduces T_g by 6°C, while changing the interface distribution in the material does not apparently affect T_g. During isothermal aging, the nanocomposites display two mechanisms toward equilibrium in a short time scale, differing from bulk PMMA. The introduction of NPs greatly increases the aging rate of PMMA, enabling the material to display two mechanisms within a shorter time scale. After the formation of NP pillars induced by the electric field, the aging rate and enthalpy recovery demonstrate a significant reduction from the nanocomposites with NPs uniformly distributed, while the aging mechanism does not fundamentally change. The hypothesis of the free volume holes' migration can be adapted to explain these findings. Reduced aging speed of polymer nanocomposites with NP alignments improves stability of such materials in their applications, further endeavor may be focused on materials selection and design to optimize the effect with consideration of specific conditions in applications.

AUTHOR CONTRIBUTIONS

Miao Huo: Investigation (lead); writing – original draft (lead); writing – review and editing (supporting). **Mingchao Ma:** Investigation (supporting); methodology (supporting); writing – review and editing (supporting). **Yinuo Teng:** Investigation (supporting); writing – review and editing (supporting). **Yuhan Xiao:** Investigation (supporting); methodology (supporting); writing – review and editing (supporting). **Yunlong Guo:** Conceptualization (lead); methodology (lead); project administration (lead); resources (lead); supervision (lead); writing – review and editing (lead).

DATA AVAILABILITY STATEMENT

The data that support the findings of this study are available from the corresponding author upon reasonable request.

ORCID

Yunlong Guo https://orcid.org/0000-0002-4490-2140

REFERENCES

[1] A. M. Rao, E. Richter, S. Bandow, B. Chase, P. C. Eklund, K. A. Williams, S. Fang, K. R. Subbaswamy, M. Menon, A. Thess, R. E. Smalley, G. Dresselhaus, M. S. Dresselhaus, *Science* **1997**, *275*, 187.
[2] T. Ramanathan, F. T. Fisher, R. S. Ruoff, L. C. Brinson, *Chem. Mater.* **2005**, *17*, 1290.
[3] E. A. Appel, M. W. Tibbitt, M. J. Webber, B. A. Mattix, O. Veiseh, R. Langer, *Nat. Commun.* **2015**, *6*, 6295.
[4] G. Schmidt, M. M. Malwitz, *Curr. Opin. Colloid Interface Sci.* **2003**, *8*, 103.
[5] D. Cangialosi, V. M. Boucher, A. Alegría, J. Colmenero, *Polymer* **2012**, *53*, 1362.
[6] A. L. Flory, T. Ramanathan, L. C. Brinson, *Macromolecules* **2010**, *43*, 4247.
[7] V. M. Boucher, D. Cangialosi, A. Alegría, J. Colmenero, J. González-Irun, L. M. Liz-Marzan, *Soft Matter* **2010**, *6*, 3306.
[8] I. M. Hodge, *Science* **1995**, *267*, 1945.
[9] D. Cangialosi, V. M. Boucher, A. Alegría, J. Colmenero, *Soft Matter* **2013**, *9*, 8619.
[10] P. Rittigstein, J. M. Torkelson, *J. Polym. Sci., Part B: Polym. Phys.* **2006**, *44*, 2935.
[11] V. M. Boucher, D. Cangialosi, A. Alegría, J. Colmenero, *Phys. Chem. Chem. Phys.* **2017**, *19*, 961.
[12] S. L. Simon, in *Encyclopedia of Polymer Science and Technology*, Vol. 1, John Wiley & Sons, Inc.Hoboken, New Jersey **2002**.
[13] C. A. Angell, *J. Non-Cryst. Solids* **1991**, *131-133*, 13.
[14] P. Rittigstein, R. D. Priestley, L. J. Broadbelt, J. M. Torkelson, *Nat. Mater.* **2007**, *6*, 278.
[15] J. M. Torkelson, R. D. Priestley, P. Rittigstein, M. K. Mundra, C. B. Roth, *Novel Effects of Confinement and Interfaces on the Glass Transition Temperature and Physical Aging in Polymer Films and Nanocomposites*. AIP Conference Proceedings, American Institute of Physics, Melville, New York **2008**, p. 192.
[16] Y. Guo, C. Zhang, C. Lai, R. D. Priestley, M. D'Acunzi, G. Fytas, *ACS Nano* **2011**, *5*, 5365.
[17] D. S. Langhe, T. M. Murphy, A. Shaver, C. LaPorte, B. Freeman, D. Paul, E. Baer, *Polymer* **2012**, *53*, 1925.
[18] V. M. Boucher, D. Cangialosi, A. Alegría, J. Colmenero, I. Pastoriza-Santos, L. M. Liz-Marzan, *Soft Matter* **2011**, *7*, 3607.
[19] M. Huo, M. Ma, Y. Guo, *ACS Appl. Polym. Mater.* **2020**, *2*, 3411.
[20] C. Liedel, K. A. Schindler, M. J. Pavan, C. Lewin, C. W. Pester, M. Ruppel, V. S. Urban, R. Shenhar, A. Böker, *Small* **2013**, *9*, 3276.
[21] K. Amundson, E. Helfand, D. D. Davis, X. Quan, S. S. Patel, S. D. Smith, *Macromolecules* **1991**, *24*, 6546.
[22] L. Berberich, M. Bell, *J. Appl. Phys.* **1940**, *11*, 681.
[23] L. M. Clayton, A. K. Sikder, A. Kumar, M. Cinke, M. Meyyappan, T. G. Gerasimov, J. P. Harmon, *Adv. Funct. Mater.* **2005**, *15*, 101.
[24] Q. Li, S. L. Simon, *Polymer* **2006**, *47*, 4781.
[25] I. Echeverria, P.-C. Su, S. L. Simon, D. J. Plazek, *J. Polym. Sci., Part B: Polym. Phys.* **1995**, *33*, 2457.
[26] I. M. Hodge, A. R. Berens, *Macromolecules* **1982**, *15*, 762.

[27] K. Niss, J. C. Dyre, T. Hecksher, *J. Chem. Phys.* **2020**, *152*, 041103.
[28] R. Svoboda, J. Málek, *J. Non-Cryst. Solids* **2013**, *378*, 186.
[29] J. Gómez Ribelles, M. Monleón Pradas, *Macromolecules* **1995**, *28*, 5867.
[30] H. N. Ritland, *J. Am. Ceram. Soc.* **1956**, *39*, 403.
[31] H. G. Ock, K. H. Ahn, S. J. Lee, *J. Appl. Polym. Sci.* **2016**, *133*, 133 (25).
[32] X. Zhou, S. Zhang, W. Huebner, P. Ownby, H. Gu, *J. Mater. Sci.* **2001**, *36*, 3759.
[33] S. Batra, M. Cakmak, *Nanoscale* **2015**, *7*, 20571.
[34] Y. H. Roos, S. Drusch, *Phase Transitions in Foods*, Academic Press, Cambridge, Massachusetts **2015**.
[35] C. Ribeiro, J. Zimeri, E. Yildiz, J. Kokini, *Carbohydr. Polym.* **2003**, *51*, 273.
[36] A. Bansal, H. Yang, C. Li, B. C. Benicewicz, S. K. Kumar, L. S. Schadler, *J. Polym. Sci., Part B: Polym. Phys.* **2006**, *44*, 2944.
[37] R. Greiner, F. R. Schwarzl, *Rheol. Acta* **1984**, *23*, 378.
[38] D. Cangialosi, V. M. Boucher, A. Alegría, J. Colmenero, *J. Chem. Phys.* **2011**, *135*, 014901.
[39] V. M. Boucher, D. Cangialosi, A. Alegría, J. Colmenero, *J. Chem. Phys.* **2017**, *146*, 203312.
[40] M. Ma, Y. Guo, *J. Polym. Sci.* **2021**, *59*, 300.
[41] D. Cangialosi, V. M. Boucher, A. Alegría, J. Colmenero, *Phys. Rev. Lett.* **2013**, *111*, 095701.
[42] V. M. Boucher, D. Cangialosi, A. Alegría, J. Colmenero, *Macromolecules* **2011**, *44*, 8333.
[43] D. Cangialosi, A. Alegría, J. Colmenero, in *Fast Scanning Calorimetry* (Eds: C. Schick, V. Mathot), Springer International Publishing, Cham **2016**, p. 403.
[44] V. M. Boucher, D. Cangialosi, A. Alegría, J. Colmenero, *Macromolecules* **2012**, *45*, 5296.
[45] M. S. McCaig, D. R. Paul, J. W. Barlow, *Polymer* **2000**, *41*, 639.
[46] A. W. Thornton, A. J. Hill, *Ind. Eng. Chem. Res.* **2010**, *49*, 12119.
[47] V. M. Boucher, D. Cangialosi, A. Alegría, J. Colmenero, *Thermochim. Acta* **2014**, *575*, 233.
[48] L. Berthier, M. D. Ediger. Facets of glass physics. arXiv Preprint *arXiv:1512.03540* **2015**.
[49] D. Cangialosi, M. Wübbenhorst, J. Groenewold, E. Mendes, H. Schut, A. Van Veen, S. Picken, *Phys. Rev. B* **2004**, *70*, 224213.

SUPPORTING INFORMATION

Additional supporting information can be found online in the Supporting Information section at the end of this article.

How to cite this article: M. Huo, M. Ma, Y. Teng, Y. Xiao, Y. Guo, *J. Appl. Polym. Sci.* **2023**, *140*(28), e54030. https://doi.org/10.1002/app.54030